Hypersonic Shocks: the Role of Radiation

C. Stehlé[1], M. Kozlová[2], J. Larour[3], J. Nejdl[2], N. Champion[1], P. Barroso[4], F. Suzuki-Vidal[5], O. Acef[6], P.-A. Delattre[1], J. Dostál[2], M. Krus[2], J.-P. Chièze[7]

1 LERMA, UMR 8112, Observatoire de Paris, UPMC, CNRS, 5 Place J. Janssen, 92195 Meudon, France
2 Institute of Physics of ASCR, Na Slovance 2, 182 21 Prague 8, Czech Republic
3 Laboratoire de Physique des Plasmas, UMR 7648, Ecole Polytechnique, UPMC, CNRS, 91128 Palaiseau, France
4 GEPI, UMR 8111, Observatoire de Paris, Paris Diderot, CNRS, 5, place Jules Janssen, 92195 Meudon, France
5 The Blackett Laboratory, Imperial College, Prince Consort Road, London SW7 2AZ, UK
6 SYRTE, UMR8630, Observatoire de Paris, UMPC, CNRS, 61, Av. de l'Observatoire, 75014 Paris, France
7 IRFU/Service d'Astrophysique, CEA-Saclay, 91191 Gif sur Yvette, France

Email contact of main author: chantal.stehle@obspm.fr

Abstract. Producing radiative shocks is known to be feasible using high-energy laser installations. Radiative shocks are characterized by an ionization front induced by the shock wave. For a given shock velocity, which is set by the available laser energy, and a given initial gas pressure, the radiative effects are more important for a high atomic number. It is why we use xenon for such objective. A laser fluence of 10^{14} W/cm^2 is sufficient to drive a shock wave at an initial velocity of about 60 km/s. The role played together by opacity and geometry is critical for the physics of these shock waves. Moreover, radiation is an obvious way of probing the shock waves, either by self-emission or by probe absorption. These aspects will be illustrated by recent experimental results obtained at the iodine PALS (Prague Asterix Laser System) laser facility in Prague.

1. Introduction

Our motivation is mainly to understand the physics of shock waves occurring during stellar formation, when Young Stars accrete matter from surrounding circumstellar environment. Accretion is often associated to dramatic hydrodynamical signatures such as collimated jets and strong radiative shocks, which are characteristic features seen in star-forming regions. The excess luminosity and X ray spectral signatures recorded by space observatories, and resulting from the accretion shocks, are used to estimate the accretion rate. Such flows have very complex structures, and drastic modelling approximations have been used so far, oversimplifying the geometry or neglecting the coupling between radiation and hydrodynamics. Thus, accretion rates are uncertain by up to a factor of 10 and the picture of star formation's basic process remains rather sketchy. In particular, the efficiency of the jet launching mechanism and the impact of accretion on stellar contraction are still not well understood. In the prevailing scenario, the accretion flows on Young Stars are supposed to follow cylindrical accretion funnels connecting the stellar photosphere to the disk along the lines of the magnetic field [1]. Even in such a configuration, there is not a clear consensus on the location of the shock wave, either in the chromosphere or in the deeper photosphere. However, depending on the location, the effect of radiation trapping is different and thus the structure of the shock and its signatures may differ. These difficulties justify the present efforts to improve the modelling of these shock waves with up to date multidimensional hydrodynamical codes and radiative transfer post-processing. In this context, experiments allow to improve the knowledge of these hypersonic flows in regimes similar to the astrophysical cases, and also to compare experimental results with codes, which, in return, will be used for modelling astrophysical shocks.

The experimental study of strong radiative shock waves in gases has been stimulated within the last 10 years by the availability of kJ laser installations, allowing to launch shock waves with velocities between 50 and 130 km/s and to study the coupling between radiation and hydrodynamics in simple geometries [2-6]. Besides astrophysical applications, the topic is of interest for fusion plasmas, the entry of various bodies in the Earth or planetary atmospheres and in various astrophysical circumstances.

By radiative shock, we mean a very strong shock wave, in which the shock front is heated at a very high temperature and thus presents a strong self-emission. Depending on the opacity, the photons emitted from this zone might be reabsorbed by the cold gas in which the shock propagates. This generates a noticeable ionisation wave, also called a radiative precursor [2, 7, 8, 9]. The complexity of the physical description of these flows, which results from the radiation effects [10], is enhanced by the non-ideal effects in the gas (e.g. ionisation, equation of state ...) [11] and by the geometrical effects even in cylindrical or parallelepipedic shock tubes [11-13].

The typical setup of experimental shock waves consists in a 1D geometry, i.e. cylindrical or parallelepipedic shock tubes (mm scale) filled with Xenon at low pressure. The laser beam is then focused on a foil, which acts as a piston. In our experiment, as in previous ones, we used a structured foil consisting in 10 μm of polystyrene followed by a thin layer of gold (0.5 μm). The ablation of the polystyrene by the laser generates the shock wave, which travels through the gold layer acting as a radiation shield, preventing the X rays induced by ablation to preheat the Xenon inside the cell. An irradiance of 1.5 10^{14} W/cm^2 (60 J, diameter of the focal spot equal to 400 μm, pulse duration 0.3 ns, corresponding to the PALS laser conditions, [14]) allows to launch highly hypersonic shock waves at velocities of about 60 km/s [4, 5]).

Most of the experiments have focused on the study of the radiative precursor, e.g. by using optical laser probing (shadowgraphy and interferometry) [2,4,5]. Hard X-ray backlighting has been used at Rochester [3,6] to image the shock front. From these types of studies, several points can be highlighted: (i) radiation cooling strongly affects the geometry and temperature of the precursor, (ii) the interactions between the shock and the walls of the gas cell may be appreciable [6], (iii) the shock wave may be observed at late times (~ 40 ns) in a regime where the velocities of the ionisation and shock fronts are comparable [5]. However, none of these experiments were able to probe the whole shock structure, i.e. the precursor, the shock front and the post-shock. Moreover, the study of the radiative signatures of these shocks remain very challenging [5]. The experiments presented here aim at testing the feasibility of two new diagnostics: instantaneous imaging of the whole shock structure with an auxiliary X-ray laser (XRL) at 21.2 nm and a photometric, spatially resolved, study of the plasma self-emission which will also be useful to follow the shock chronometry.

In the following, we shall first point out what is the role played by radiation in the experimental shock wave. Then the experimental setup and results obtained at PALS laser facility [14,15] will be presented.

2. Radiation effects

In the adiabatic limit and for mono-atomic gases, hypersonic shock waves can reach temperatures up to

$$T \sim 3/16\ \mu/k\ D^2$$

Where D is the shock velocity and μ the mean molecular weight of the plasma. Thus gases having higher atomic masses are more favourable to radiation effects scaling in power of the temperature. In the typical experimental case, the shock velocity is equal to 60 km/s and the gas is xenon at a fraction of 1 bar. Hereafter, we shall fix the initial pressure to 0.3 bar, as it corresponds to the experimental results. One expects to reach ion temperatures up to ~ 1000 eV in the adiabatic limit. Due to electronic excitation and ionisation, the temperature is lower and reaches ~ 20 eV for Xenon in previous conditions. Similarly, the compression ratio varies from 4 for a perfect gas, up to 13 for real gases and more when radiation is taken into account.

Typical snapshots of the temperature, mass and electron densities and Xenon ionic charge are reported in Figure 1. The 1D simulations [16] include the coupling between radiation and hydrodynamics and are performed with the experimental conditions, i.e. 1.5 x 10^{14} W/cm^2 of the PALS laser beam (~ 0.3 ns) working in the infrared. The snapshots were obtained at 11 ns after the laser arrival. The distance is reported from the interface Xe-Au, thus only the xenon conditions are given. The effect of radiation appears if one compares these results with those obtained with the same setup, except that radiation effects are not included (figure 2). The shapes of the curves are quite different. The compression is smaller, the shock velocity larger and the temperature decreases slowly towards the colder gold layer. The more spectacular effect is the absence of radiative precursor

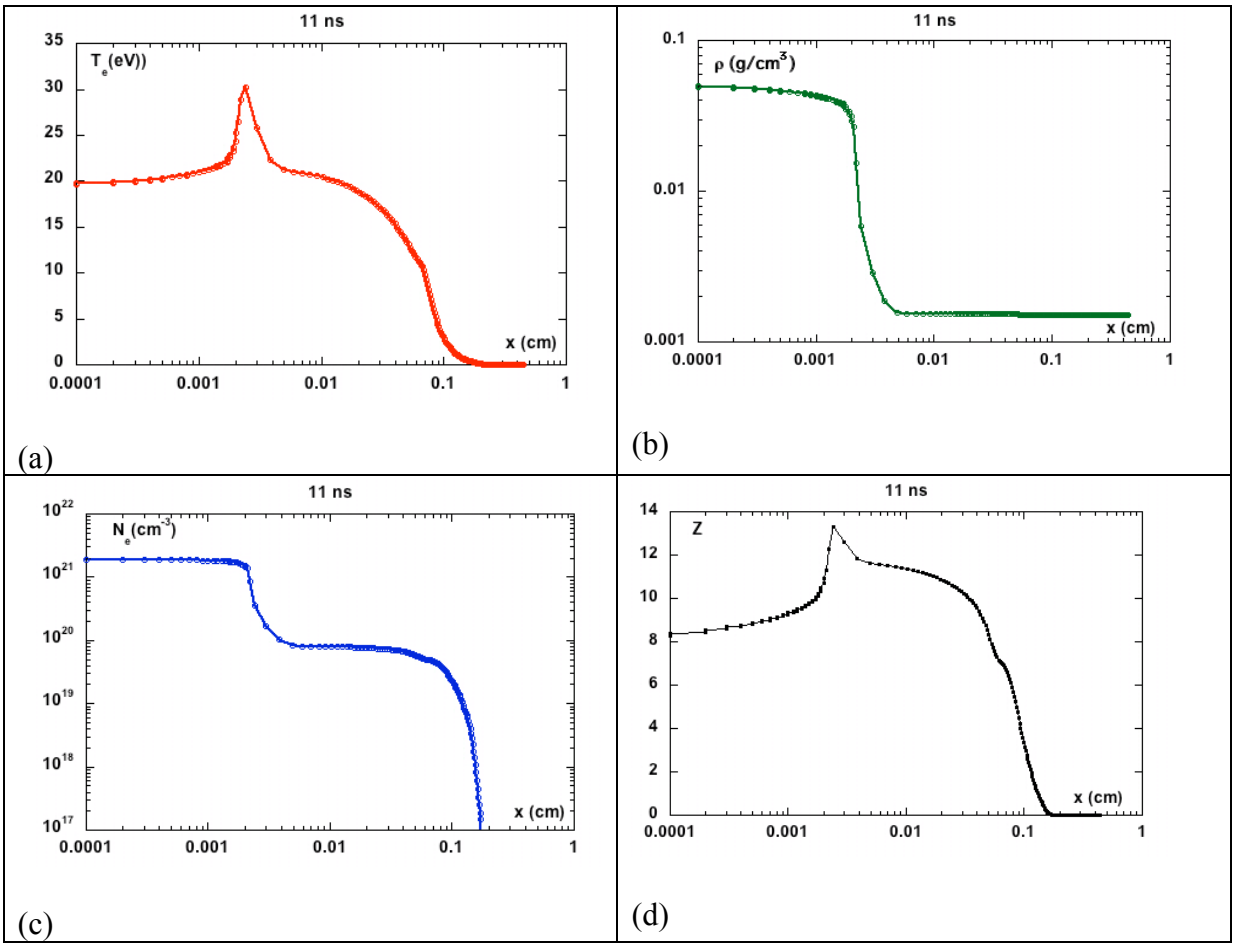

Figure 1: Snapshot at 11 ns after laser arrival on the target of the temperature, mass density, electron density and mean ion charge for Xenon (0.3 bar) in the experimental conditions. The origin (x=0) corresponds to the Au-Xe interface..

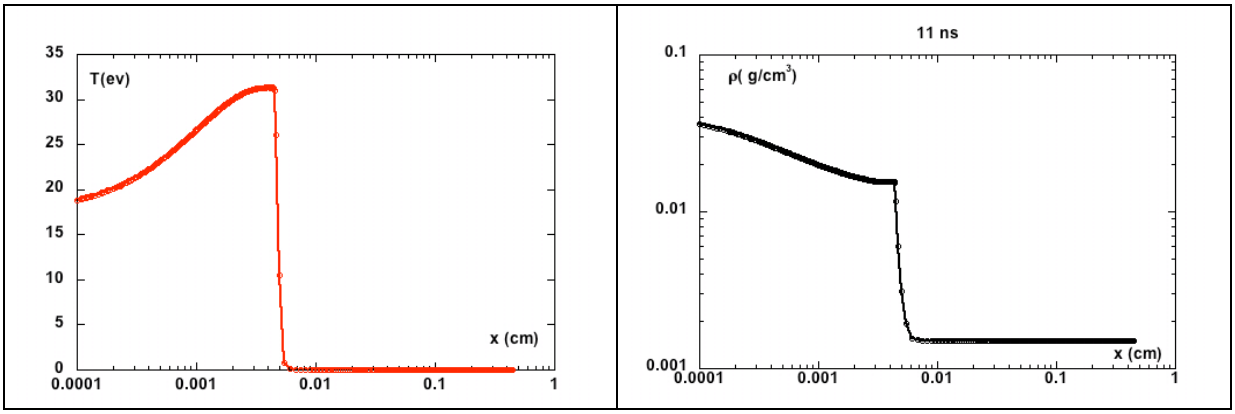

Figure 2: same as Figure 1. The radiation effects are not included in the simulation.

Another effect of the radiation concerns the boundary conditions: the shock tube has a finite section. Thus the 1D simulations for the shock may only be used for shock tube experiments in the limit case of fully reflective specular reflexion of radiation on the walls. However, the XUV emission from a radiation front having a temperature of 30 eV (and even less), may be

absorbed by the walls, thus no longer effective to ionize the precursor. This effect has been suspected from experiments with shock velocities of about 60 km/s [2, 4, 5] and confirmed later on by numerical simulations performed by a 2-D radiative hydrodynamic code [17]. As a consequence, the precursor extension is smaller, the ionising front is bent and the time needed to reach a quasi-stationary limit is reduced. This last aspect has been explored in recent experiment on the PALS laser [5] in the same velocity range and confirmed by simulations. At higher velocities, the interaction between radiation and the walls is stronger, as shown by experiments performed at about 130 km/s (1 bar) [6].

3. Experimental setup

The experiments were conducted at the Prague Asterix Laser System (PALS) [14,15]. The core of the experimental setup (Figure 3) consists of two beams from the IR iodine laser, with a pulse duration of 0.3 ns. The first beam (hereafter called AUX beam, 60 J) drives the shock wave inside a target filled with Xenon (at 0.3 bar). The second beam (hereafter called MAIN beam, 500 J) generates an XUV laser beam at 21.2 nm (hereafter called XRL beam). In terms of diagnostics, the XRL beam is used as a back-lighter of the shock wave, with a controlled delay of 20 ns after AUX beam, allowing the instantaneous imaging of the shock. The second main diagnostic consists of a set of high-speed silicon diodes recording the plasma self-emission at a given position of the shock tube. Finally, an X-ray pinhole camera monitors the energy distribution of the AUX laser beam on the target.

The targets used for the shock generation consist in a "shock tube" of section 0.4 x 0.4 mm^2, length 6 mm, closed by a piston made from a gilt polystyrene (CH) (Figure 4). The AUX beam is focused on the polystyrene foil (thickness 10 μm) by an f =100 cm lens, yielding an irradiance of ~ 1 -2 x 10^{14} W/cm^2 on a spot of diameter ~ 0.4 mm. The CH ablation propels the piston inside the shock tube at an expected velocity in the range of 50-60 km/s. For the XUV backlighting, as for plasma self emission diagnostics, we used 150 nm thick Si3N4 windows (length of 3 mm, width of 0.4 mm). A post-mortem inspection of the targets allows controlling the centring of the AUX beam on the target.

The XRL beam at 21.2 nm is generated in a spherical vacuum chamber from a plasma column with a length of ~ 30 mm by the sequence of a low intensity infrared prepulse (loosely focused ~ 700 μm) and the strong MAIN pulse (tightly focus ~ 150 μm) on an optically polished Zn slab. By using the half-cavity configuration, the XRL delivers up to a 10-mJ in a 150-ps pulse with a divergence of about 4 x 6 mrd^2 [18,19]. The XRL beam propagates through the shock -target, and is reflected by a spherical Mo/Si multilayer mirror (f= 300 mm); it passes through a pinhole located in the focal plane of the mirror and reaches a cooled CCD camera located at the position of the image of the shock tube through this mirror, with a magnification of 8.4. The iron pinhole (500 μm diameter) acts as a spatial filter to improve the contrast on the CCD of the XRL versus the strong plasma self-emission [20]. Moreover, the intense visible stray light of the plasma is filtered by a 0.4 μm thick self-supported Aluminium foil.

A high-speed 1-mm^2 Silicon bare diode is located perpendicularly to the longitudinal axis of the shock tube to record the time dependent self-emission of the plasma. The diode is located at ~ 55 mm from the lateral window of the target with an angle of 30 degrees with respect to the horizontal plane in order to allow the XRL beam to pass through the windows. The spatial

resolution is ensured by a Tungsten slit (thickness 50 microns, section 0.175 x 0.4 mm^2) located at 9.5 mm from the window. The slit orientation is perpendicular to the longitudinal axis of the tube along which the shock propagates. The rise-time of the diode (0.7 ns) is compatible with high quality coaxial cables, 3 GHz bandwidth bias tees and attenuators. The time response of the detection chain is adapted to the study of a mm-thick shock travelling at 60km/s. The slit aperture gives for this velocity a 5 ns time window.

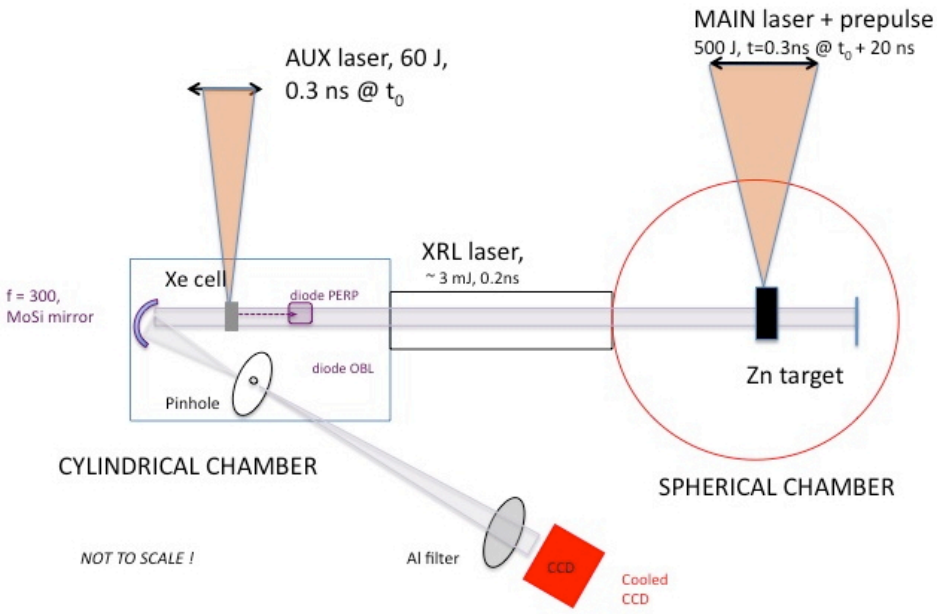

Figure 3: Schematic experimental setup showing the two main laser beams (MAIN and AUX), which drive respectively the XRL probe beam and a radiative shock inside a Xe-filled gas tube. The XUV imaging and diode diagnostics are also reported.

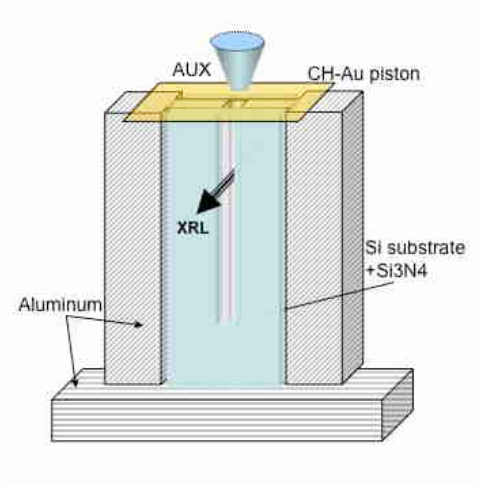

Figure 4: scheme of the target. AUX laser is coming from the top and is focalized on the piston, whereas XRL laser goes through the Si3N4 windows.

4. Results

Monochromatic radiography with X-ray laser offers several advantages compared to other

techniques: the number of photons, a parallel beam, and the possibility to probe dense matter up to a fraction of the corresponding electron critical density (2.5 x 10^{24} cm^{-3}). The technique is expected to probe the dense part of the shock, and also the heated low-density precursor, where absorption occurs through the rich spectral signatures of the moderately charged Xenon ions in the VUV [17- 20]. The expected structure of the plasma at 20 ns, during the XRL pulse, reported in Figure 5, using 1D simulations [16], presents a maximum electron density up to 10^{21} cm^{-3} in Xenon and 10^{23} cm^{-3} in gold. The thickness of the shocked Xenon layer is approximately equal to 10 µm (i.e. 6 pixels expected on the CCD), which is of the same order of magnitude than the blurring due to the motion of the shock wave during the 0.15 ns of the XRL laser.

The Figure 6 shows the image of the plasma at 21 nm. The initial position of the piston (Au/CH layer) is close to the right border of the image. The AUX laser (~ 60 J) comes from the right. The relatively low number of counts (50-100 after subtraction of the image background) is due to various factors: the geometric losses, as only a fraction of the XRL beam passes through the target; the strong absorption of XRL laser light by the two Si3N4 windows closing the target (transmission of 0.15%); losses at the Mo-Si mirror (~ 30% at 21 nm) and through the Aluminium filter (50%) shielding the CCD [21]. The unexpected static speckles on the record are attributed to the low surface quality of the commercial substrate of the spherical imaging MoSi mirror.

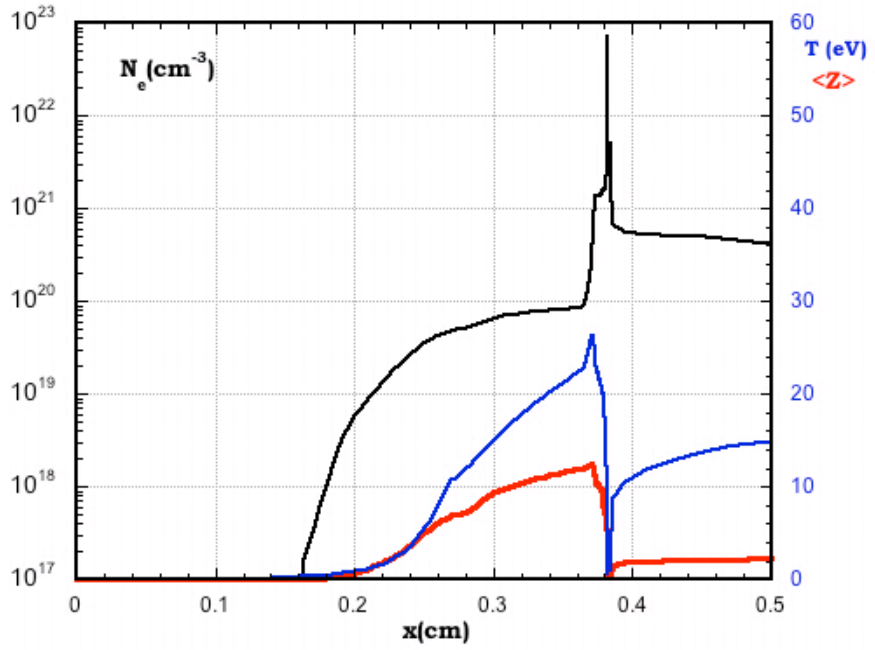

Figure 5: Snapshot of the plasma at 20 ns from 1D simulations [16]. The initial position of the piston is at x = 0.5 cm and the laser is coming from the right. The position of the shock front in xenon is located at 0.37 cm. The electron density peaks at 1.4 10^{21} cm^{-3}, the electron temperature at 26 eV and the mean ion stage at 13. The Xe-Au interface is at 0.386 cm and the CH-Au interface is located at 0.382 cm.

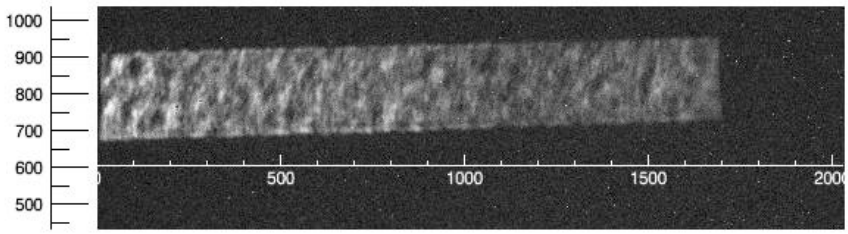

Figure 6: Image at 20 ns after its launching of a shock located close to the middle of the picture (x ~1000-1300 pixels). The delay between XRL and AUX is set to 20 ns.

However as the noisy patterns present a negligible shot-to-shot displacement, it is possible to perform the division of the image with a reference image without shock wave. The resulting synthetic (ratio) image, presented in Figure 7, is then the transmission of the plasma at 21.2 nm and at 20 ns after the arrival of AUX on the target. The shock wave is located around pixel 1100, where the transmission is at minimum, i.e. 1.5 mm from the initial position. This is slightly larger by 0.15 mm than the position expected from the simulation, which remains reasonable. Due to the typical scale of the noisy patterns, it becomes difficult to assess that the darker small structures (thickness ~ 10 pixels) close to this position come from the shocked Xenon or gold. It is interesting to note that the hottest part of the precursor (between pixels 800 and 1100, i.e. about 100 µm in the target) absorbs the XRL radiation. This is expected from the rich line spectrum in the XUV range of warm Xenon [22-24]. Behind the shock (pixel number larger than 1100), the image remains dark in a zone which, in 1-D, is attributed to hot CH and should present a marginal absorption. The darkening is then more pronounced close to the walls (i.e. ~ y = 900 and y= 650 pixels) and could be attributed to the walls being heated by the shock. Whereas 1-D simulations predict that a negligible absorption after the gold layer in the expanding CH and no emission neither for gold nor for CH, an important absorption remains on the CCD (x ~ 1100- 1700 pixels in Figure 7) .

The shock velocity estimated from the XRL probing is confirmed by the plasma self-emission registered by the fast diode which recorded the plasma self-emission coming from a section of the shock tube located at ~ 2.2 mm from initial position of the piston, and with an emitting surface of about 0.2 x 0.4 mm^2. The diode was not filtered and no analogical attenuators were used on it. The resulting record is reported in Figure 8. We observe a strong peak at time t = 0, which is attributed to stray light during the intense interaction between AUX and the CH-Au foil. Moreover, a slight electrical echo is observed at ~15 ns, which is attributed to an impedance mismatch of the coaxial feed-through at the chamber wall. The signal from the diode increases after 20 ns, reaching a maximum at ~ 40 ns. This maximum is followed by a slow decrease reaching a plateau and a secondary peak at ~ 80 ns. The peak temperature (~ 24 eV in 1-D simulation) is reached when the shock front appears in the window. The expected corresponding theoretical signal (blackbody radiation assumption) shows a maximum in the emissivity at ~ 36 ns, which is close to the measured value. The timing obtained in the simulation is close to the experimental value of 40 ns (Figure 8).

Concerning the peak intensity (front shock), XUV imaging at 20 ns and self-emission at 2-2.2 mm, these results are consistent with a shock wave propagating at ~ 60 km/s. Contrary to qualitative estimation (using blackbody emission of the plasma), the emission remains important after the time of arrival of shock front (36 ns). This effect, which is coherent with the opacity at 21 nm after the shock itself, could be eventually attributed to the heated windows or to some Xenon, which has been entrained in the shock.

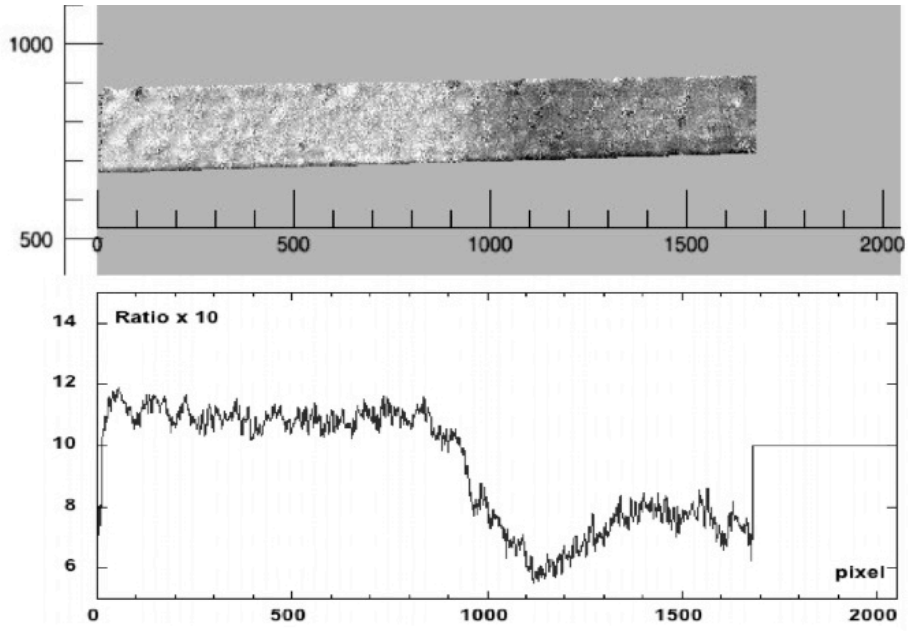

Figure 7: Upper image: ratio (multiplied by 11) of two images, one with and the other without shock. The image is smoothed over 20 pixels. Lower image: mean value of the ratio (arbitrarily multiplied by 10) over the 200 pixels of the vertical section of the upper image.

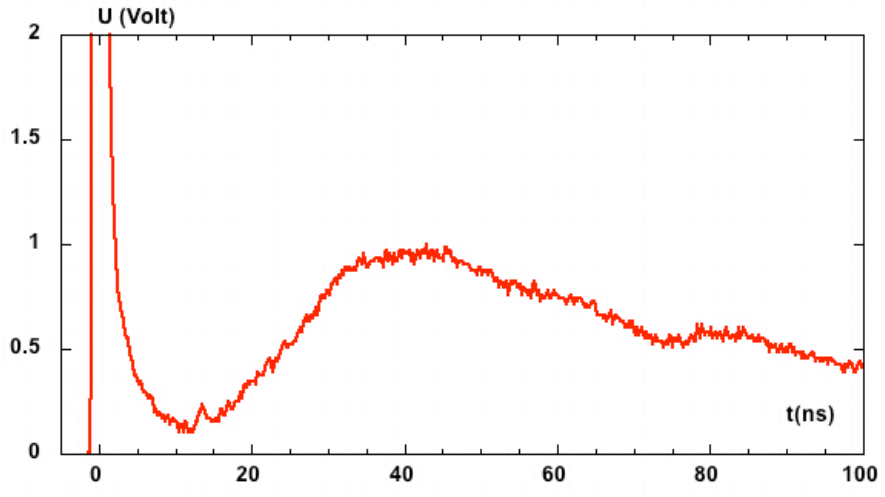

Figure 8: Signal of the photodiode in Volt versus time in ns. The maximum at ~ 36 ns corresponds to the time of arrival of the shock front.

5. Conclusions

We present the first experimental study of radiative shock waves in gases by simultaneous XRL imaging and spatially resolved plasma self-emission. The results obtained by both diagnostics are consistent and in qualitative agreement with the chronometry expected from 1-D simulations. XRL backlighting allows probing not only the shock front but also a part of the radiative precursor. Using high quality imaging mirrors, this XRL diagnostic will allow visualizing departures from 1-D behaviour, as for instance the precursor bending or the heating of the shock tube. As the mass density in the radiative precursor is equal to that of the unperturbed Xenon, it is important to point out that the XRL probing would theoretically allow measuring the

temperature, supposing the opacity at 21 nm correctly known from theory or from other dedicated experimental studies. Concerning the diode diagnostics, the present result opens a door to more detailed studies, using for instance diodes with various filtering to improve the evaluation of the temperature of the emitting plasma. Future studies will take benefit from 2D hydro-simulations and 3D radiative transfer post-processing.

6. Acknowledgements

The authors acknowledge the vital contributions of the PALS technical team, the target fabrication team of Observatoire de Paris, the important contribution of V. Petitbon at IPN for the piston manufacturing, and illuminating discussions with F. Delmotte and S. de Rossi (Institut d'Optique, University Paris Sud-Orsay), B. Rus (Institute of Physics in Prague), F. Delahaye, A. Ciardi (LERMA), M. Gonzalez (IRFU). The work was supported by LASERLAB access program, French ANR, under grant 08-BLAN-0263-07, PICS4343 of CNRS, by University Pierre et Marie Curie and Observatoire de Paris. This work was partially supported by the Academy of Sciences of the Czech Republic (Project No. M100100911), by the Czech Ministry of Education, Youth and Sports (Project Nos. 7E08099 and 7E09092), and by the Czech Science Foundation (Grant No. 202/08/1734).

7. References

[1] BOUVIER, J., et al. (2007), "Magnetospheric Accretion in Classical T Tauri Stars", in Protostars and Planets V, B. Reipurth, D. Jewitt, and K. Keil (eds.), University of Arizona Press, Tucson, p. 479-494, (arXiv:astro-ph/0603498)

[2] BOUQUET, S., et al. (2004), « Observations of laser driven supercritical radiative shock precursors », *Phys. Rev. Lett.* **92** 5001

[3] REIGHARD, A.B., et al., (2006), « Observation of collapsing radiative shocks in laboratory experiments », Physics of Plasmas, 13, 082901

[4] GONZÁLEZ, M., et al., (2006), "Astrophysical radiative shocks : from modelling to laboratory experiments", *Laser Part. Beams,* **24**, 535-545

[5] STEHLE, C., et al., « Experimental Study of Radiative Shocks at PALS facility », (2010), *Laser Part. Beams*, **28,** 253.

[6] DOSS, F.W., et al. (2009), « Wall shocks in High-energy-density shock tube experiments », *Phys. of Plasmas*, **16**, 112705.

[7] Y.B. ZELDOVICH, Y.P. RAIZER, (1996), « Physics of shock waves and high temperature hydrodynamic phenomena », New York: Academic Press.

[8] PENZO, A., TASSART, J. (1984),« Establishement of a supercritical shock-wave in the piston model », *Journal de Mécanique Théorique et Appliquée*, **3**, 381.

[9] KISELEV, YU N., et al. Mathematical modelling of the propagation of intensely radiating shock waves, *Comput. Maths. Math. Phys.,* **31**, No.6, pp.87-101

[10] BOUQUET, S. et al.,(2000), « Analytical study and structure of a quasistationnary radiative shock », *Astroph. J Supp.*, **127,** 245.

[11] MICHAUT, C., et al., (2004), "Jump conditions in hypersonic shocks. Quantitative effects of ionic excitation and radiation", *Eur. Phys. J. D*, **28,** 381-392

[12] LEYGNAC, S. et al., (2006), « Modeling multidimensional effects in the propagation of radiative shocks », *Phys. of Plasmas* **, 13**, 113301.

[13] GONZÁLEZ, M., et al., (2009), « 2D numerical study of the radiation influence on shock structure relevant to laboratory astrophysics » , *A&A* **, 497**, 27-34

[14] JUNGWIRTH, K. et al., (2001), « The Prague Asterix Laser System », *Physics of Plasmas,* **8**, 2495.

[15] BATANI, D, et al., (2007), "Recent experiments on the hydrodynamics of laser-produced plasmas conducted at the PALS laboratory", *Laser and Particle Beams*, **25**, 127.

[16] RAMIS, R., et al., (1988) « MULTI – a computer code for onedimensional multigroup radiation hydrodynamics », *Comp. Phys. Comm*., **49**, 475.

[17] GONZÁLEZ, M., et al., (2007), « HERACLES: a three dimensional radiation hydrodynamics code», *A&A,* **464**, 429-435

[18] RUS, B., et al. , (2002), « Multi-millijoule, deeply saturated x-ray laser at 21.2 nm for applications in plasma physics », *Plasma Phys. Control. Fusion*, **44**, B207

[19] RUS, B., et al. (2002) « Multi-millijoule, highly coherent x-ray laser at 21.2 nm operating in deep saturation through double-pass amplification », *Phys. Rev. A* **66**, 063806.

[20] KOZLOVÁ, M. ,et al., (2009), « High Resolution X-ray Laser Backlighting of Plasmas Using Spatial Filtering Technique », in X-Ray Lasers 2008, Proceedings Book Series: Springer Proceedings in Physics, **130,** 417.

[21] HENKE, B.L., et al. (1993), « X-ray interactions: photoabsorption, scattering, transmission, and reflection at E=50-30000 eV, Z=1-92 », *Atomic Data and Nuclear Data Tables*, **54** (no.2), 181.

[22] FIEDOROWICZ, H., et al. , (1999), « Investigation of soft X-ray emission from a gas puff target irradiated with a Nd:YAG laser », *Optics Comm*., 163 , 103.

[23] KIEFT, E.R., et al., (2005) « Comparison of experimental and simulated extreme ultraviolet spectra of xenon and tin discharges », *Phys. Rev. E*, 71, 036402.

[24] J. BLACKBURN, et al., (1983), « Spectra of Xe-VII, Xe-VIII, and Xe-IX in the Extreme Ultraviolet – 4d-mp, nf transitions », *Journal of Optical Society of America*, **73**, 1325.